Pharm Res (2014) 31:2988–3005
DOI 10.1007/s11095-014-1393-4

RESEARCH PAPER

Hyaluronan-Based Nanocarriers with CD44-Overexpressed Cancer Cell Targeting

Shuangshuang Song • Huan Qi • Jingwen Xu • Pan Guo • Fen Chen • Fei Li • Xinggang Yang • Naicheng Sheng • Yingliang Wu • Weisan Pan

Received: 30 December 2013 / Accepted: 15 April 2014 / Published online: 20 May 2014

ABSTRACT

Purpose The objective of the work was to evaluate the potential of hyaluronan-based nanoparticles as tumor-targeting nanosystems for CD44-overexpressed cancer therapy.

Methods The synthesized amphiphilic cholesteryl succinoyl hyaluronan (Chol-Suc-HA) conjugates self-assembled into docetaxel(DTX)-loaded nanoparticles in the aqueous environment. The physiochemical properties of Chol-Suc-HA-DTX NPs were characterized. The *in vitro* cytotoxicity of Chol-Suc-HA-DTX NPs against MCF-7, 4T1, A549 and L929 cells was evaluated using MTT and LDH assays. Moreover, the cellular uptake mechanism was investigated using the CLSM and flow cytometry. The *in vivo* animal experiments of Chol-Suc-HA-DTX NPs including pharmacokinetic evaluation, bio-distribution observed by *EX vivo* NIRF imaging and antitumor efficacy were also carried out in SD rats or 4T1 tumor-bearing BALB/c mice.

Results The self-assembled Chol-Suc-HA-DTX NPs with different degree of substitution (DS) of hydrophobic moiety exhibited high drug loading, uniform particle size distribution and excellent *in vitro* stability. However, the plasma stability of Chol-Suc-HA-DTX NPs was significantly influenced by the DS of hydrophobic moiety. The higher the DS was, the more stable the NPs were. Cellular uptake demonstrated that Chol-Suc-HA-DTX NPs were internalized into cancer cells via CD44 receptor-mediated endocytosis. Compared with Taxotere®, Chol-Suc-HA-DTX NPs displayed remarkably higher cytotoxicity to CD44-positive cancer cells (MCF-7, 4T1, A549 cells). *In vivo* animal experiments confirmed that Chol-Suc-HA-DTX NPs with relatively high DS values exhibited prolonged circulation time, excellent tumor-targeting properties and efficient antitumor effects with extremely low systemic toxicity. In addition, blank Chol-Suc-HA NPs also slightly suppressed the tumor growth.

Conclusions Chol-Suc-HA NPs with a suitable DS value portend to be promising drug vehicles for systemic targeting of CD44-overexpressed cancers.

KEY WORDS CD44-mediated endocytosis · hyaluronan · interference with endogenous HA-CD44 interaction · tumor-targeting

ABBREVIATIONS

4T1	Mice mammary cancer cells
A549	Non-small lung cancer cells
C6	Coumarin-6
CHEMS	Cholesteryl hemisuccinate
CLSM	Confocal laser scanning microscope
DCC	N,N′-dicyclohexylcarbodiimide
DCM	Dichloromethane
DL	Drug loading
DLS	Dynamic light scattering
DMAP	4-dimethylaminopyridine
DMEM	Dulbecco's modified eagle medium
DS	Degree of substitution
DTX	Docetaxel
ECM	Extracellular matrix
EE	Entrapment efficiency
HA	Hyaluronan
HAS	HA synthase
Hyals	Hyaluronidases
L929	Mice fibroblasts
LDH	Lactate dehydrogenase

S. Song • P. Guo • F. Chen • F. Li • X. Yang • W. Pan (✉)
School of Pharmacy, Shenyang Pharmaceutical University, PO Box No. 122, 103 Wenhua Road, Shenyang 110016, People's Republic of China
e-mail: pwstfzy@163.com

H. Qi • J. Xu • Y. Wu (✉)
College of Life Science and Biopharmaceutical, Shenyang Pharmaceutical University, PO Box No. 122, 103 Wenhua Road, Shenyang 110016, People's Republic of China
e-mail: yingliang1016@163.com

N. Sheng
Institute of Metal Research, University of Chinese Academy of Sciences, 72 Wenhua Road, Shenyang 110016, China

MCF-7	Human breast cancer cells
MTT	3-(4,5-dimethyl-thiazol-2-yl)-2,5-diphenyl-tetrazoliumbromide
NIRF	Near infrared fluorescence
RAW 264.7	Murine macrophage cells
TEM	Transmission electron microscopy
TIR	Tumor inhibition rate

INTRODUCTION

A significant obstacle that needs to be overcome for improving therapeutic index of anticancer chemotherapy is the lack of site-specific accumulation in tumor sites, which results in severe side effects and therefore restricts the clinical application for the treatment of various cancers (1–4). Such nonselective distribution of antitumor drugs in the whole body has promoted the development of tumor-targeted nano-scale drug delivery system which could improve the selective cytotoxicity of anticancer drugs to the tumor tissues and reduce drug exposure to the normal tissues. During the last decades, increasing efforts have been placed on the self-assembled polymeric nanoparticles functionalized with a variety of tumor-targeting ligands, such as transferrin (5), folate (6), peptides (7), antibody fragments (8) and so on, due to their powerful advantage in targeting drugs to the tumor sites via passive as well as active mechanisms (9–11).

Hyaluronan (HA), also called Hyaluronic acid, is a linear and negatively charged glycosaminoglycan polymer composed of repeating disaccharide units of glucuronic acid and N-acetylglucosamine (12,13). HA with variable polymer length is synthesized by transmembrane HA synthases (HAS1, HAS2 and HAS3) on the inner surface of cell membrane and secreted into the extracellular matrix (ECM) (14,15). High-molecular-size HA polymers existing in ECM are degraded into the smaller-size fragments mainly by two types of hyaluronidases (Hyal-1 and Hyal-2) after binding to CD44 receptors on the surface of cells. (16–18). CD44 is a transmembrane glycoprotein which is over-expressed in many types of cancerous cells such as breast, lung, colorectal, and melanoma cancer cells and all CD44 isoforms contain a HA-binding site in their extracellular region. Therefore, CD44 is the major receptor for extracellular HA (19). Interestingly, a number of recent studies have associated CD44-HA interaction with tumor progression and metastasis (20–23). Interfering with CD44-HA interaction by exogenous HA or anti-CD44 antibody can impair the tumor growth and metastasis (24,25). Consequently, HA and CD44 are both potential therapeutic targets for the treatment of cancers. Yoshihara S *et al.* reported that the HAS inhibitor, 4-methylumbelliferone, inhibited growth of melanoma cells and metastasis to other organs (26). The study performed by Zeng C *et al.* indicated that subcutaneous administration of exogenous HA oligomers markedly inhibited local tumor growth (27). Other strategies including inhibition of CD44-HA interaction with soluble recombinant CD44 and application of Hyals to reduce interstitial fluid pressure caused by HA layers have also achieved good anticancer efficacy (28,29). Therefore, disruption of endogenous HA-CD44 interaction may be a potentially useful adjuvant therapy for conventional anticancer drugs. In recent years, combination of chemotherapeutic drugs with HA-based nanocarriers for selectively targeting CD44-overexpressed cancer cells has received increasing attention. HA-based nano-particulate systems with various structure such as HA-drug conjugates (30,31), self-assembled HA nanoparticles (32–35), and HA–decorated nanoparticles (36,37) have been extensively investigated owing to their efficient drug loading, excellent colloidal stability and prolonged circulation in blood, and preferential drug accumulation in the tumor sites. In our previous study, we successfully developed a hyaluronic acid-coated docetaxel-loaded cholesteryl hemisuccinate vesicles (HA-CHEMS vesicles) (38). Compared to commercial Taxotere®, HA-CHEMS vesicles significantly enhanced the antitumor efficacy and reduced the systemic toxicity of docetaxel. However, the mechanism of HA coating on CHEMS vesicles was electrostatic interaction between the negatively charged HA and positively charged CHEMS vesicles, so the issue of whether part of the HA might dissociate from the surface of CHEMS vesicles and cleared from the blood after systemic administration remains to be proved.

In order to eliminate the concern, in the current work, we have synthesized a novel amphiphilic HA derivative, in which hydrophilic HA was grafted with cholesteryl hemisuccinate (CHEMS). The hydrophobically modified HA could self-assemble into unique nanoparticles with a hydrophobic inner-core and a hydrophilic outer-shell in the aqueous environment. On the one hand, once HA-based nanoparticles carried the anticancer drugs to the CD44-overexpressed tumor sites, the nanoparticles would bind to the CD44 receptor, forming caveolae. As the caveolae became endosomes and finally fused with lysosomes, the HA outer-shell was degraded mainly by Hyal-1, resulting in drug release. On the other hand, HA outer-shell of nanoparticles as exogenous HA could interfere with endogenous HA-CD44 interaction, leading to a better tumor response as a potential adjuvant therapy (Scheme 1).

MATERIALS AND METHODS

Materials

HA with an average molecular weight of 7.62 kDa was provided by Shandong Freda Biopharm Co. Ltd. (Shandong, China). Succinic anhydride were kindly supplied by China National Medicine Corporation LTD. (Shanghai, China). 3-(4,5-dimethyl-thiazol-2-yl)-2,5-diphenyl-tetrazoliumbromide (MTT), N,N′-

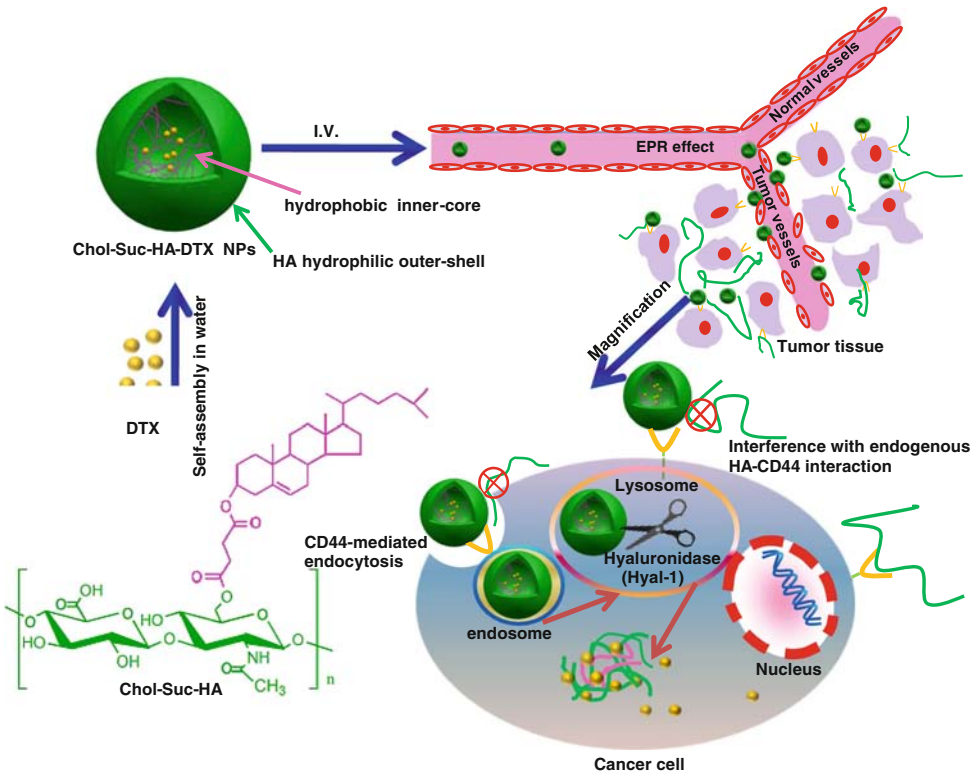

Scheme I Schematic illustration of the self-assembly, accumulation at the tumor site and internalization into the cancer cells of Chol-Suc-HA-DTX NPs.

dicyclohexylcarbodiimide (DCC), 4-dimethylaminopyridine (DMAP), pyridine, cholesterol and coumarin-6 were obtained from Sigma–Aldrich Co. (St. Louis, MO, USA). Hoechst 33342 was purchased from Molecular Probes (Eugene, OR). DiR was purchased from Beyotime® Biotechnology Co. Ltd (Jiangsu, China). Docetaxel (DTX) was offered by Jiangsu Hengrui Pharmaceutical Co. Ltd. (Jiangsu, China). Commercial docetaxel solution (Taxotere®) was purchased from Sanofi Aventis (France). All other chemicals and reagents used were of analytical grade, obtained commercially.

Synthesis of Chol-Suc-HA Conjugates

The Chol-Suc-HA conjugates were synthesized by the following two-step procedure as illustrated in Scheme 2.

Synthesis of Cholesteryl Hemisuccinate (CHEMS)

CHEMS was synthesized according to the previously described method with a slight modification (39). Briefly, 7.732 g of cholesterol (20 mmol) and 2.006 g of succinic anhydride (20 mmol) were dissolved in 40 ml of anhydrous dichloromethane (DCM) in a three-necked flask equipped with a reflux condenser. Then, 10 ml of pyridine was added and the reaction mixture was stirred magnetically in an oil bath at 65°C for 3 days under reflux. Thereafter, the DCM was removed by a rotary evaporator under vacuum. The obtained residues were dissolved in 50 ml of acetone at 55°C, followed by filtration to remove the insoluble matter. The filtrate was stored at −20°C overnight. The resultant precipitate was re-dissolved in 20 ml of chloroform to further remove the insoluble matter, followed by filtration and rotary evaluation. The procedure was repeated twice. The final product was further purified by silica gel column chromatography (For detailed purification procedure, please see the supplementary material). After the purification process, the product CHEMS resulted as a white solid. Yield: 60–65% (gravimetric). The molecular weight of CHEMS determined by ESI-MS was 486.3. The ^{1}H-NMR spectra of CHEMS was recorded on a Bruker AV-400 MHz spectrometer using $CDCl_3$ as the solvent.

Synthesis of Cholesteryl Hemisuccinate-Grafted Hyaluronan (Chol-Suc-HA Conjugates)

The hydrophobic CHEMS was covalently conjugated to the HA backbone by esterification reaction. In brief, various amounts of CHEMS together with DMAP (1.2 mol/mol CHEMS) and DCC (1.2 mol/mol CHEMS) were dissolved in 10 ml of DMSO at 65°C and stirred for 4 h to activate the carboxyl groups. One hundred milligrams of HA (0.26 mmol, the number of moles of C6′–OH as shown in Fig. 1c) were added to 10 ml of formamide and completely dissolved by mild stirring at 65°C. Then, the HA solution was slowly added into the above solution, followed by reaction for 48 h at 65°C under argon gas. After 48 h, the mixture was filtered and the resultant

Scheme 2 Synthetic scheme of Chol-Suc-HA conjugate.

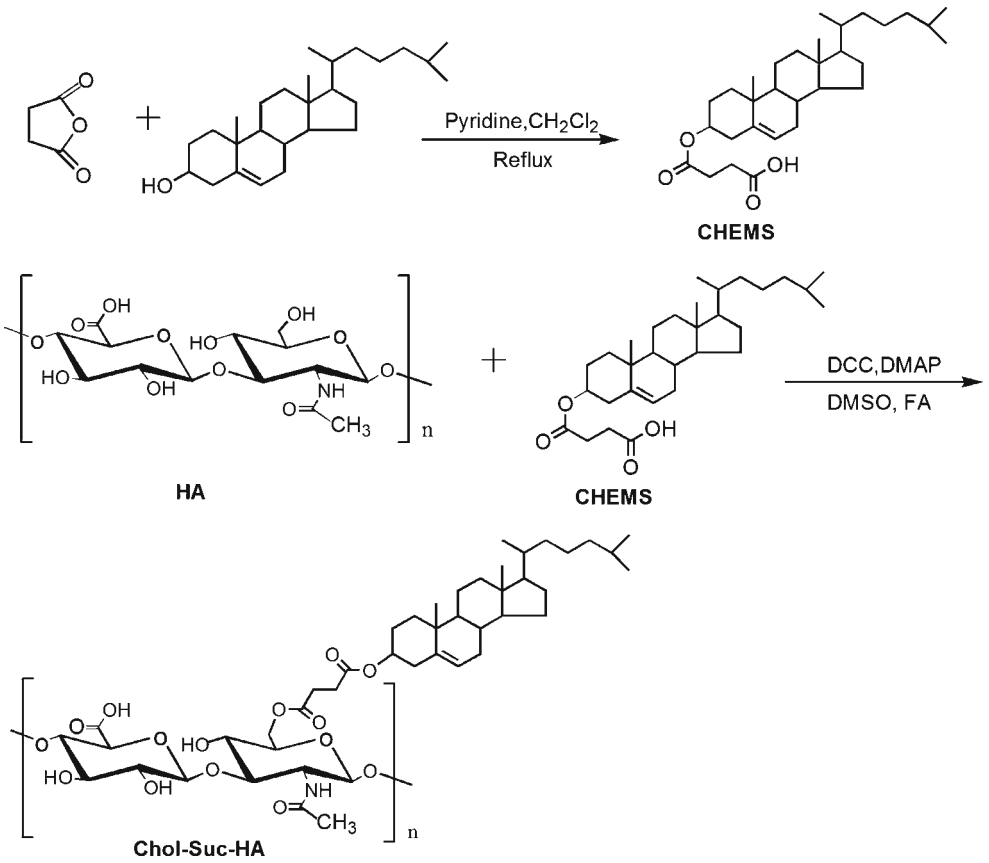

filtrate was dialyzed against excess amount of ethanol/distilled water solution (85:15, *v*/*v*), ethanol/distilled water solution (50:50, *v*/*v*) and distilled water, each for 2 days. The medium was exchanged frequently. Finally, the dialyzed solution was centrifuged at 2000 rpm for 15 min to remove other impurities. The supernatant was lyophilized to obtain the white product. The binding of CHEMS to hydrophilic HA backbone was confirmed by the characteristic peaks of CHEMS appearing in the ^{1}H-NMR spectra of Chol-Suc-HA using D_2O as the solvent. The degree of substitution (DS) of CHEMS was 8.2% (Chol-Suc-HA1), 18.3% (Chol-Suc-HA2) and 25.6% (Chol-Suc-HA3), respectively, determined by ^{1}H-NMR. The three kinds of synthesized Chol-Suc-HA conjugates were subsequently used to prepare Chol-Suc-HA nanoparticles.

Preparation and Characterization of Chol-Suc-HA-DTX NPs

Three kinds of DTX-loaded polymeric nanoparticles composed of Chol-Suc-HA conjugates were prepared using a previously described membrane dialysis method (40). Briefly, accurately weighed amounts of DTX and Chol-Suc-HA conjugates with a mass ratio of 1/8 was dissolved in 1 ml of DMSO and then was injected dropwise into 5 ml of phosphate buffer saline (PBS, pH 7.4) under mild stirring at room temperature. The obtained mixture was further dialyzed against PBS (pH 7.4) for 24 h using a dialysis bag (MWCO: 8–10 kDa). Thereafter, the self-assembled DTX-loaded Chol-Suc-HA nanoparticles (Chol-Suc-HA-DTX NPs) dispersion was condensed to 5 ml, where the concentration of Chol-Suc-HA conjugates was 0.8% wt, in a water bath at 65°C and subsequently sonicated with a ultrasonic cell crusher at 100 W for 5 min (1 s pulse and 2 s rest). In order to completely remove the non-encapsulated drug, the nanoparticles dispersion was centrifuged at 3000 rpm for 15 min, and filtered using the 0.45 μm microfiltration membrane. The theoretical drug concentration should be 1 mg/ml. However, the unentrapped drug was removed via filtration, so the final drug concentration in the dispersion measured using HPLC was 0.88, 0.94 and 0.96 mg/ml for Chol-Suc-HA1-DTX NPs, Chol-Suc-HA2-DTX NPs and Chol-Suc-HA3-DTX NPs, respectively. The three kinds of Chol-Suc-HA-DTX NPs dispersions were directly used for subsequent experiments. In order to store the NPs for a long time, the Chol-Suc-HA-DTX NPs dispersion could be lyophilized using 3% mannitol as lyoprotectants (For the detailed conditions of freeze drying, please see the supplementary material).

The particle size and zeta potential of Chol-Suc-HA-DTX NPs were measured by dynamic light scattering (DLS) analysis using a Zetasizer Nano ZS90 instrument (Malvern, UK) with a scattering angle of 90° at 25°C. The morphology of NPs was observed by the transmission electron microscopy (TEM)

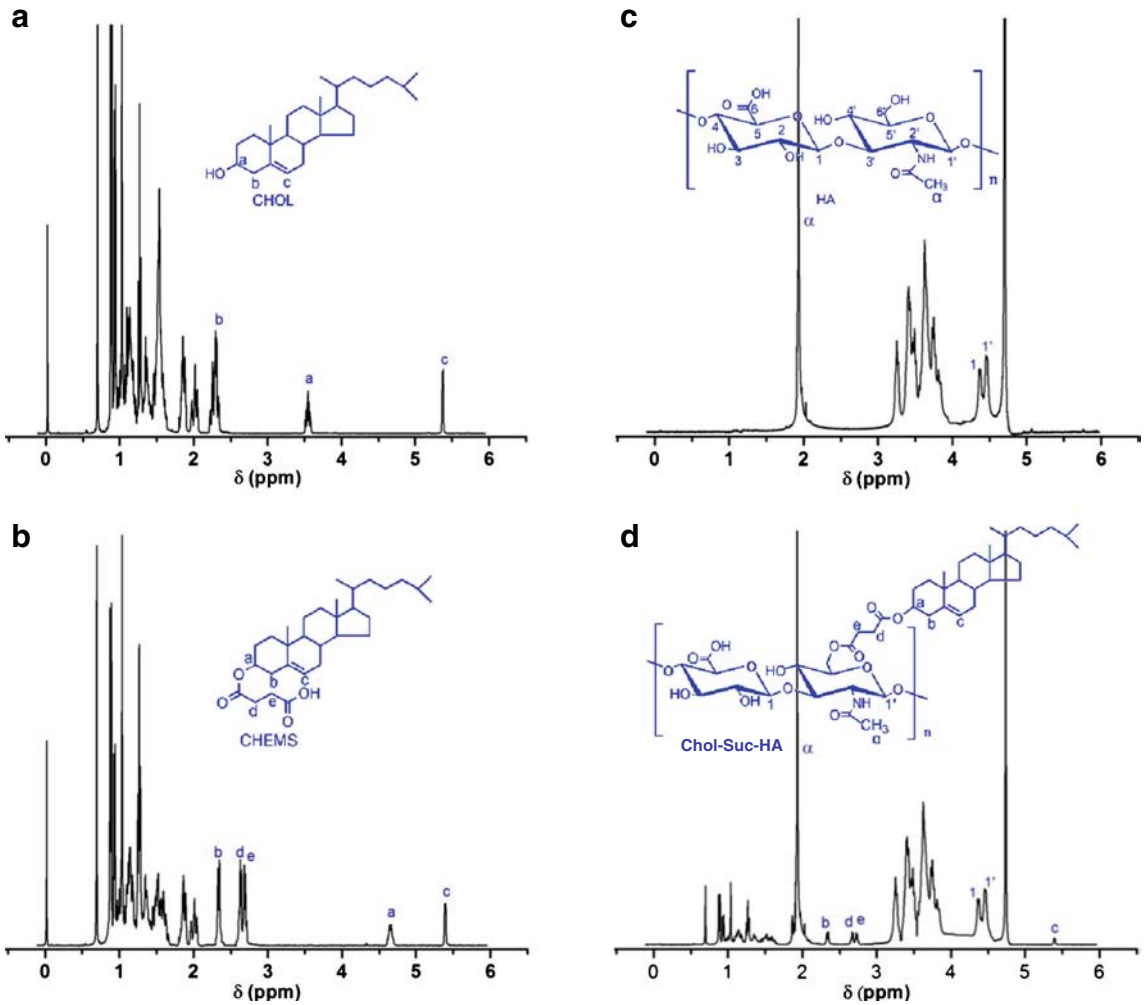

Fig. 1 ^{1}H NMR spectra of (**a**) CHOL and (**b**) CHEMS in $CDCl_3$, (**c**) HA and (**d**) Chol-Suc-HA in D_2O.

(JEM-1200EX, JEOL, Japan) after negative staining (The detailed process was in the supplementary material). In addition, the stability of Chol-Suc-HA-DTX NPs dispersion at room temperature and 4°C was monitored by measuring the change of particle size.

For the measurement of entrapment efficiency (EE) and drug loading (DL), 0.2 ml of Chol-Suc-HA-DTX NPs dispersion prepared as described above was mixed with 9.8 ml of DMSO, followed by sonication disruption for 15 min and centrifugation for 10 min at 8000 rpm. The DTX content in the supernatant was assayed by HPLC as described previously (38). The EE and DL was calculated using the following formulas:

$$EE(\%) = \frac{amount\ \ of\ \ DTX\ \ in\ \ NPs}{amount\ \ of\ \ the\ feeding\ \ DTX} \times 100$$

$$DL(\%) = \frac{amount\ \ of\ \ DTX\ \ in\ \ NPs}{amount\ \ of\ \ NPs} \times 100$$

In Vitro Release of CHOL-SUC-HA-DTX NPs

In vitro release of DTX from Taxotere® and Chol-Suc-HA NPs was performed using the dialysis bag method. In brief, 1 ml of different DTX dispersions (the drug concentration in Chol-Suc-HA1 NPs, Chol-Suc-HA2 NPs, Chol-Suc-HA3 NPs and Taxotere® was 0.88, 0.94, 0.96 and 1.01 mg/ml, respectively) was sealed in a dialysis bag (MWCO: 8–10 kDa) and immersed into 30 ml of PBS (pH 7.4) containing 0.5% Tween80. The entire system was kept at 37°C under continuous shaking (100 rpm). At predetermined time points, 100 μl of release medium was withdrawn and replenished with an equivalent volume of fresh medium. The medium was centrifuged at 8000 rpm for 10 min and the DTX content in the supernatant was determined by HPLC (see supplementary material). The release profile was plotted as a function of time. In order to investigate if Hyal-1 has an effect on the release behavior of Chol-Suc-HA-DTX NPs, the drug release from Chol-Suc-HA3 NPs was performed in acetate buffer (pH 4.2) containing 0.5% Tween80 and different enzyme activity of Hyal-1.

The Integrity and Stability Studies of Chol-Suc-HA-DTX NPs in Plasma

The integrity of Chol-Suc-HA-DTX NPs during incubation with rat plasma for 24 h was evaluated by determining the content of DTX retained in the NPs. In brief, 1 ml of different Chol-Suc-HA-DTX NPs dispersions (the drug concentration in Chol-Suc-HA1 NPs, Chol-Suc-HA2 NPs and Chol-Suc-HA3 NPs was 0.88, 0.94 and 0.96 mg/ml, respectively) was mixed with a certain volume of rat plasma which had been filtered through 0.22 μm microfiltration membrane and incubated at 37°C for 24 h. At designed time points, 100 μl of mixture was taken out and centrifuged at 3000 rpm for 10 min to remove the leaked DTX. The supernatant was mixed with 300 μl of acetonitrile, then vortexed for 10 min and finally centrifuged at 10000 rpm for 10 min. The amount of DTX retained in the NPs was measured by the HPLC (see the supplementary material). Moreover, the colloidal stability of NPs when dispersed in rat plasma was also estimated. After the NPs dispersion was centrifuged at 3000 rpm for 10 min, the time-dependent change in particle size was measured by DLS.

Cell Culture

RAW 264.7 murine macrophage cells, MCF-7 human breast cancer cells, 4T1 mice mammary cancer cells, A549 non-small lung cancer cells and L929 mice fibroblasts were purchased from Type Culture Collection of Chinese Academy of Sciences (Shanghai, China) and cultured in DMEM or RPMI 1640 medium supplemented with 10% fetal bovine serum, 100 U/ml streptomycin, and 100 U/ml penicillin G in a humidified atmosphere of 5% CO_2 at 37°C. The expression level of CD44 on the surface of MCF-7, 4T1 and A549 cells was significantly higher than that on the surface of L929 (data not shown).

In Vitro Cytotoxicity

A comparison of cytotoxicity of Chol-Suc-HA-DTX NPs and Taxotere® was performed in MCF-7, 4T1, A549 and L929 cell lines. Two hundred microliters of cell suspension at a density of 4×10^4 cell/ml was seeded into a 96-well plate and grew for 24 h before treatment. Then, the medium was removed and the cells were washed three times. Following exposure to different DTX formulations diluted to various drug concentrations with culture medium for 72 h, the supernatant was aspirated and centrifuged at 500 rpm for 10 min. The activity of LDH was assayed using a standard LDH release kit (Sigma, TOX7-1KT). The LDH release was presented as percentage of control values which were obtained by measuring the LDH activity releasing from the untreated cells. Meanwhile, 180 μl of culture medium and 20 μl of MTT solution (5 mg/ml) was added to the 96-well plate and incubated for another 4 h. After that, the medium was removed and 200 μl of DMSO was added for dissolving the formazan crystals. Absorbance was measured at 570 nm using a BioRed microplate reader (Model 500, USA). Cell viability was expressed as a percentage relative to the absorbance of untreated cells. Moreover, the growth inhibitory concentration for 50% of the cell population (IC_{50}) was calculated by regression of the cell viability data.

In Vitro Cell Uptake

Cellular Internalization

Confocal Microscopy. In order to track the *in vitro* cellular uptake, hydrophobic fluorescence dye coumarin-6 (C6) instead of DTX was encapsulated into the Chol-Suc-HA NPs. The entrapment efficiency of three kinds of C6-loaded Chol-Suc-HA (Chol-Suc-HA-C6) NPs was 99.2±0.7%, 99.5±0.5% and 99.8±1.1%, respectively. The final C6 concentration in three kinds of Chol-Suc-HA-C6 NPs dispersions was 39.7, 39.8 and 39.9 μg/ml. Cellular internalization property of Chol-Suc-HA-C6 NPs was observed by a confocal laser scanning microscope (CLSM). MCF-7, 4T1 or A549 cells at a density of 2×10^5/well were seeded onto a 6-well plate with a sterile coverslip and cultured for 24 h. Thereafter, the medium was replaced with serum-free culture medium containing free C6 or Chol-Suc-HA-C6 NPs (2 μg/ml). After 2 h incubation period, the cells were washed three times with cold PBS (pH 7.4) and fixed with 4% paraformaldehyde in PBS (pH 7.4) for 10 min. Then, the cells were washed three times and the nuclei were stained with Hoechst 33342 at 37°C for 30 min in the darkness. Finally, the fixed cell monolayer was washed thrice with PBS and mounted using glycerol. The coverslip was observed using a CLSM (LSM 710, Carl Zeiss, Germany).

Flow Cytometry. The flow cytometry was employed to quantitatively measure the fluorescence intensity in the cancer cells treated with free C6 and Chol-Suc-HA-C6 NPs (2 μg/ml). After incubation with above formulations for 2 h, the cells were washed three times with PBS (pH 7.4) and re-dispersed in PBS for flow cytometry analysis (Becton Dickinson, Germany). 10,000 events were collected for all samples.

Investigation on Mechanism of Cellular Uptake

The cellular uptake mechanism was investigated by cell uptake experiment at 4°C, the competitive inhibition study using free HA (10 mg/ml), and negative control of L929 cells. For the competitive inhibition study, the cells were treated with HA solution for 30 min prior to incubation with Chol-Suc-

HA-C6 NPs. Other experimental procedures were performed as described above.

The Impact of HA as Hydrophilic Outer-Shell on the Opsonization and Macrophage Uptake

To explore whether the HA hydrophilic outer-shell can impair the opsonization in the bloodstream and uptake of Chol-Suc-HA NPs by macrophages, the extent of nanoparticles uptake by RAW 264.7 cells was quantified by flow cytometry. Briefly, an aliquot of Chol-Suc-HA-C6 NPs was directly incubated with RAW 264.7 cells or first incubated with rat plasma (10 or 30 min) before being exposed to the RAW 264.7 cells. After 2 h incubation, the cells were washed three times with PBS (pH 7.4) and re-dispersed in PBS. The percentage of fluorescence cells was determined by flow cytometry analysis. As a positive control, the same protocol was applied for the nude CHEMS vesicles with a hydrophobic and positively charged surface as prepared in our previous study (38).

In Vivo Study

Animals and Tumor Model

Male pathogen-free Sprague–Dawley (SD) rats (250 ± 10 g) and female BALB/c mice (20–25 g) were kindly provided by Experimental Animal Center of Shenyang Pharmaceutical University. The animals were allowed for free access to food and water and acclimatized for at least 7 days before the experiments. The *in vivo* animal experiments were conducted under the guideline approved by the Animal Care Committee at Shenyang Pharmaceutical University and followed the principles of Laboratory Animal Care (People's Republic of China). The tumor xenograft mouse model was established by injecting 1×10^6 4T1 cells in 200 μl of physiological saline into the armpit region of BALB/c mice.

In Vivo Pharmacokinetic Evaluation

SD rats were randomly divided into four groups with three in each and injected with Taxotere®, DTX-loaded Chol-Suc-HA1, Chol-Suc-HA2 and Chol-Suc-HA3 NPs via tail vein at a dose of 12.5 mg DTX/kg. At designated time points, 0.5 ml of blood samples was collected into a heparinized tube from the suborbital vein and immediately centrifuged for 10 min at 4000 rpm. The drug in the harvested plasma was extracted by deproteinization using acetonitrile, followed by centrifugation for 15 min at 12,000 rpm. The supernatant was dried under reduced pressure and re-dissolved with 100 μl of acetonitrile. The drug content was determined by HPLC (see the supplementary material).

Bio-Distribution of Chol-Suc-HA NPs Observed by Ex Vivo NIRF Imaging

The bio-distribution and tumor-targeting properties of Chol-Suc-HA NPs in 4T1 tumor-bearing BALB/c mice were evaluated using the non-invasive near-infrared optical imaging approach. The BALB/c mice with 300–400 mm^3 of tumor were subjected to NIRF imaging. 0.2 ml of DIR (near infrared fluorescence dye)-loaded Chol-Suc-HA NPs with different DS values was injected intravenously into the tumor-bearing mice at the dose of 1.5 mg DIR/kg ($n = 3$). At different time points post-injection, the mice were sacrificed and the tumors and major organs were excised, washed with physiological saline and imaged using the Kodak *in vivo* imaging system FX PRO (Carestream Health, Inc., USA) with an excitation bandpass filter at 710 nm and an emission at 790 nm. The fluorescence intensity of tumors and livers were quantified by the Kodak Molecular Imaging Software using operator-defined regions of interest (ROI).

In Vivo Antitumor Efficacy

After approximately 1-week post-inoculation, BALB/c mice bearing 50–100 mm^3 of 4T1 tumors were selected for the study on *in vivo* antitumor efficacy. The tumor-bearing BALB/c mice were randomly divided into nine groups receiving different injections ($n = 6$ in the first 6 groups and $n = 10$ in the last 3 groups) as follows: (1) i.v. injection, saline (the control group); (2) i.v. injection, Taxotere® at 10 mg DTX/kg; (3) i.v. injection, Chol-Suc-HA1-DTX NPs at 10 mg DTX/kg; (4) i.v. injection, Chol-Suc-HA2-DTX NPs at 10 mg DTX/kg; (5) i.v. injection, Chol-Suc-HA3-DTX NPs at 10 mg DTX/kg; (6) i.v. injection, blank Chol-Suc-HA3 NPs at 80 mg Chol-Suc-HA3/kg; (7) intratumoral injection, blank Chol-Suc-HA3 NPs at 80 mg Chol-Suc-HA3/kg; (8) i.v. injection, free HA solution at 80 mg HA/kg; (9) intratumoral injection, free HA solution at 80 mg HA/kg. Each group was injected every 3 days and the therapeutic effect was evaluated by measuring the tumor volume and body weight from first injection. After 24-day treatment, the mice were sacrificed and then the tumors were excised. The obtained tumors were weighed and the tumor inhibition rate (TIR) was calculated using the following formula:

$$TIR(\%) = \frac{W_{control} - W_{sample}}{W_{sample}} \times 100$$

Statistical Analysis

All Data were expressed as mean ± S.D.. Student's two-sample *t*-test and one-way ANOVA for multiple groups were used for statistical evaluation. $P < 0.05$ was considered statistically significant.

RESULTS AND DISCUSSION

Characterization of CHEMS and Chol-Suc-HA Conjugates

To synthesize Chol-Suc-HA conjugates, the hydroxyl group at C3 position of cholesterol was initially reacted with succinic anhydride to provide terminal carboxyl group. Cholesterol was selected as the hydrophobic group because of its excellent biocompatibility and non-toxicity. The assignment of chemical shifts of mainly characteristic peak was as follows ($CDCl_3$, ppm): 0.70 (3H, C18-H_3), 2.34 (2H, C4-H_2), 2.63 (2H, succinyl -CO-CH_2), 2.69 (2H, succinyl –CH_2-CO), 4.64 (1H, C3-H_1), 5.39 (1H, C6-H_1). The peaks of adjacent methylene protons appearing at 2.63 and 2.69 ppm and the change in chemical shift of the proton at C3 position from original 3.55 to 4.64 ppm confirmed the synthesis of CHEMS.

Novel amphiphilic derivatives regarded as fishbone-like polymers have been synthesized by chemical conjugation of CHEMS to HA in the presence of DCC as a coupling agent and DMAP as a catalyst. The successful grafting of CHEMS onto HA backbone was confirmed by ^{1}H-NMR as presented in Fig. 1. The proton assignment of HA was as follows (D_2O, ppm): 1.90 (3H, $NHOCH_3$), 3.0–4.0 (10H, glucosidic H), 4.34 (1H, anomeric H_1), 4.44 (1H, anomeric $H_{1'}$). Compared to HA, in the spectrum of Chol-Suc-HA, the occurrence of the characteristic peak at δ (ppm) = 0.5–2.0, 2.34, 5.39 ppm assigned to steroid rings of the cholesterol fragment and 2.70, 2.76 ppm which belong to the succinyl segment confirmed the formation of Chol-Suc-HA conjugates.

Preparation and Characterization of Chol-Suc-HA-DTX NPs

Developing novel, versatile, non-toxic and biodegradable polymeric nanoparticles that exhibit advantageous properties such as ease of preparation, high stability, prolonged circulation in bloodstream and selectively delivery of anticancer drugs to tumor tissues is urgently needed for improving therapeutic efficacy of conventional chemotherapy. In the present study, three kinds of amphiphilic Chol-Suc-HA conjugates successfully self-assembled into nanoparticles via hydrophobic interaction between the grafted CHEMS in the aqueous solution, with the particle size ranging from 93 ± 11 to 204 ± 28 nm as determined by DLS analysis (Table I). The particle size of Chol-Suc-HA-DTX NPs decreased with the increase of DS values of hydrophobic moiety. This is mainly attributed, if not entirely, to stronger hydrophobic attractive force and more compact conformation of inner core packing. The formation of Chol-Suc-HA NPs could be further confirmed by TEM imaging, where the nanoparticles were all morphologically spherical (Fig. 2a). As summarized in Table I, the zeta potentials of Chol-Suc-HA-DTX NPs were negative, indicating that hydrophilic HA outer-shells were exposed to water interface. All Chol-Suc-HA-DTX NPs displayed high encapsulation and drug loading. Especially for Chol-Suc-HA3-DTX NPs, the entrapment efficiency and drug loading were up to 96.3 ± 3.4% and 10.7 ± 0.1%, respectively. Moreover, it can be seen that the entrapment efficiency of Chol-Suc-HA-DTX NPs increased as the DS values increased, indicating that increased chemical conjugation of hydrophobic group to the HA fragment favorably facilitated the entrapment of DTX because of enhanced binding affinity between hydrophobic drug and hydrophobic inner core. As shown in Fig. 2b, the Chol-Suc-HA-DTX NPs dispersions were highly stable with no significant particle size change and visible precipitates when stored at room temperature for 15 days and at 4°C for several months (data not shown).

In Vitro Drug Release

In vitro release behavior of Taxotere® and Chol-Suc-HA-DTX NPs was performed in PBS (pH 7.4) containing 0.5% Tween80 at 37°C for 96 h. As shown in Fig. 3a, the release of DTX from Chol-Suc-HA NPs was much slower than that from Taxotere®. DTX from Taxotere® was completely released after 24 h, whereas Chol-Suc-HA1, Chol-Suc-HA2 and Chol-Suc-HA3 NPs only released 40.4, 28.7 and 25.2% of DTX, respectively, showing a sustained release behavior. Especially for Chol-Suc-HA3-DTX NPs, only 33.1% of DTX was released after 96 h, which fully guaranteed Chol-Suc-HA NPs could carrier the majority of drug to tumor sites. Furthermore, with the increase of DS of hydrophobic group, the release rate of DTX from Chol-Suc-HA NPs slowed. This may be attributed to the compact hydrophobic core and the enhanced hydrophobic interaction between DTX and hydrophobic group (41).

Table I The Physicochemical Properties and DTX Loading Parameters of Chol-Suc-HA-DTX NPs

Formulations	Feed ratio[a]	DS (%)	Particle size (nm)	Zeta potential (mV)	EE (%)	DL (%)
Chol-Suc-HA1	1:3	8.2	204 ± 28	−31 ± 3	85.2 ± 2.8	9.6 ± 0.3
Chol-Suc-HA2	1:1	18.3	132 ± 15	−25 ± 1	93.5 ± 1.2	10.5 ± 0.3
Chol-Suc-HA3	5:3	25.6	93 ± 11	−18 ± 4	96.3 ± 3.4	10.7 ± 0.1

[a] Molar feed ratio of cholesteryl hemisuccinate to C6′-OH of HA polymer (CHEMS)

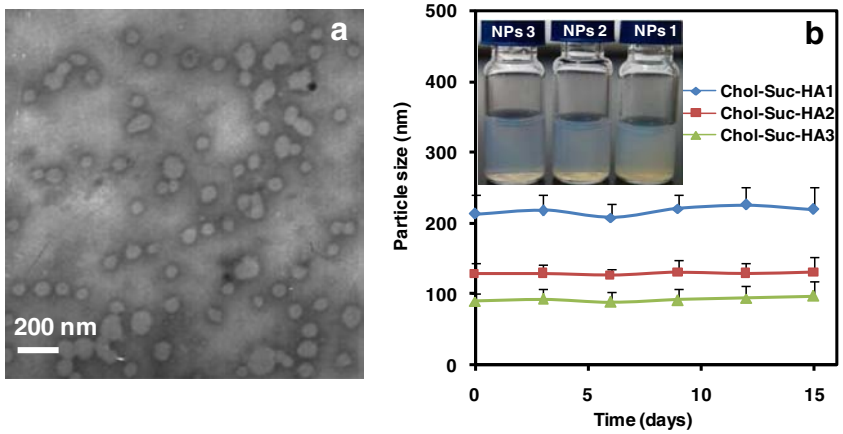

Fig. 2 (**a**) The TEM image of Chol-Suc-HA3-DTX NPs. (**b**) stability of Chol-Suc-HA-DTX NPs at room temperature evaluated by measuring the change in particle size of NPs. *Insert*: photographs of Chol-Suc-HA-DTX NPs after stored at room temperature for 15 days.

The release pattern of Chol-Suc-HA3-DTX NPs was also evaluated in acetate buffer (pH 4.2) containing different enzyme activity of Hyal-1 which is involved predominantly in degrading HA in lysosomes (42–47). As seen in Fig. 3b, the release rate of DTX from Chol-Suc-HA3 NPs accelerated with the enhancement of the enzyme activity. When the enzyme activity in acetate buffer (pH 4.2) was up to 100 U/ml, the Chol-Suc-HA3-DTX NPs displayed a significantly rapid release behavior. About 92.1% of DTX from Chol-Suc-HA3 NPs was released in 12 h, while the release of drug reached only about 23.7% in the absence of Hyal-1. This suggested that once the Chol-Suc-HA-DTX NPs were internalized into tumor cells and finally fused with lysosomes, the HA backbone could be degraded by Hyal-1, resulting in rapid drug release.

The Integrity and Stability Studies of Chol-Suc-HA-DTX NPs in Plasma

Maintaining the integrity and stability of self-assembled nanoparticles for a long time in plasma is the essential prerequisite for drug's reaching the tumor tissues and subsequently generating the antitumor efficacy. Therefore, the integrity and stability of Chol-Suc-HA-DTX NPs in rat plasma were investigated by measuring the content of DTX retained in the nanoparticles and change in particle size over time. As shown in Fig. 4a, the content of DTX retained in Chol-Suc-HA2 NPs and Chol-Suc-HA3 NPs was 67.4 and 70.5% after 24 h incubation, respectively. Given that the amounts of leaked DTX from Chol-Suc-HA2 NPs and Chol-Suc-HA3 NPs were similar to *in vitro* release amounts (28.7 and 25.2%), we speculated that the content of DTX retained in NPs reduced probably due to the DTX release from the nanoparticles instead of agglomeration and sedimentation of NPs in plasma. Thus, taking into account DTX release from the nanoparticles, the obtained results indicated that almost all of the nanoparticles kept their integrity in the presence of rat plasma. However, as for the Chol-Suc-HA1 NPs, only 4.3% of DTX retained in the nanoparticles after incubated with rat plasma for 4 h. After 12 h incubation, the content of DTX retained in Chol-Suc-HA1 NPs could not be detected. Given that the structure of Chol-Suc-HA1 NPs was similar to that of Chol-Suc-HA2 NPs and Chol-Suc-HA3 NPs, the only difference was that hydrophobic interaction between hydrophobic groups (CHEMS) was different, so the significantly reduced content may be ascribed to the fast disassembly of Chol-Suc-HA1 NPs in rat plasma. The similar observation was also reported by Chen *et al.* (48), in which the core-loaded molecules rapidly released from PEG-PDLLA micelles due to the loss of integrity of micelles *in vivo*. As illustrated in Fig. 4b and c, no significant change in particle size of Chol-Suc-HA2 NPs and Chol-Suc-HA3 NPs was observed during 24 h incubation

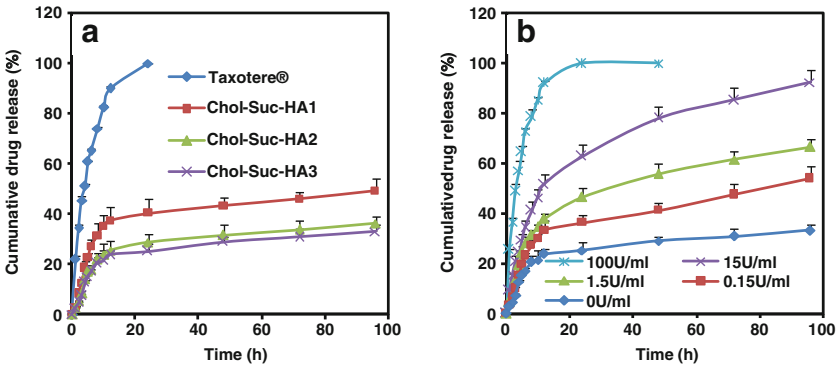

Fig. 3 (**a**) *In vitro* drug release profile of Taxotere® and Chol-Suc-HA-DTX NPs in PBS (pH 7.4). (**b**) *In vitro* release of DTX from Chol-Suc-HA3 NPs in acetate buffer (pH 4.2) containing different enzyme activity of Hyal-1 (0 U/ml, 0.15 U/ml, 1.5 U/ml, 15 U/ml, and 100 U/ml). Data represented mean ± S.D. ($n = 3$).

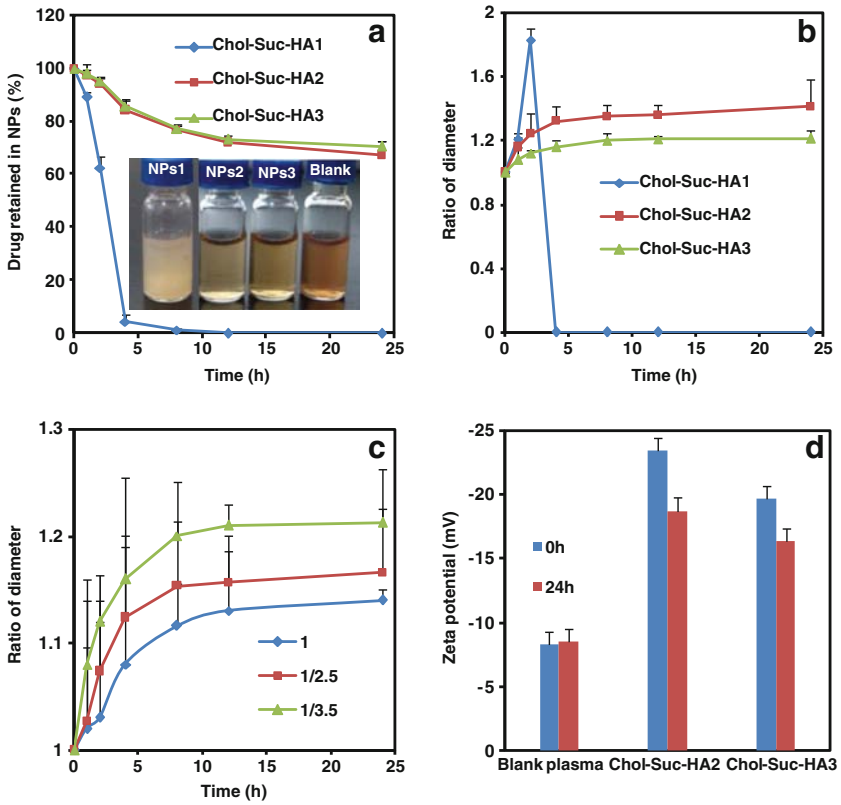

Fig. 4 (**a**) The percentage of DTX retained in Chol-Suc-HA NPs incubated with rat plasma at 1/3.5 volume ratio for different time. *Insert*: photographs of Chol-Suc-HA-DTX NPs after incubation with rat plasma at 37°C for 24 h. (**b**) Time-dependent colloidal stability of Chol-Suc-HA-DTX NPs in rat plasma at 1/3.5 volume ratio. The ratio of diameter was the ratio between the time-dependent particle size and original particle size. (**c**) Time-dependent change in particle size of Chol-Suc-HA3-DTX NPs after incubation with rat plasma at different volume ratio (1/1, 1/2.5 and 1/3.5). (**d**) Zeta potential change of Chol-Suc-HA-DTX NPs after incubation with rat plasma for 24 h at 37°C.

with rat plasma, implying no remarkable protein absorption and aggregate formation. The particle size of Chol-Suc-HA3 NPs increased with the decrease of volume ratio of nanoparticle dispersion to rat plasma ranging from 1/1 to 1/3.5 (*v*/*v*). In the case of Chol-Suc-HA1 NPs, the size change was extremely significant. It is interested to note that following centrifugation, the particle size was not detectable after 4 h incubation, further confirming that Chol-Suc-HA1 NPs encountered the structure disruption in rat plasma. From Fig. 4d, we can observe that the zeta potential of blank plasma was about −8.3 mV, which helped to reduce the protein absorption to the negatively charged Chol-Suc-HA NPs as confirmed by slight change in particle size and zeta potential. In our previous study (38), the particle size of nude CHEMS vesicles was about 4-fold higher than original particle size and the zeta potential was converted from +12.1 to −6.2 mV. The changes might be attributed to the plasma protein absorption to the positively charged surface of vesicles. Our data demonstrated that by increasing the DS values of hydrophobic moiety, the stability of self-assembled nanoparticles in plasma was significantly improved; on the other hand, HA hydrophilic outer-shell could reduce the protein absorption, hence prolonging the circulation time.

In Vitro Cytotoxicity

The LDH leakage assay based on the activity of lactate dehydrogenase releasing into the culture medium due to the cell membrane damage is widely used as an indicator of cytotoxicity. And MTT assay is another cell viability assay that could indirectly reflect the cytotoxicity following exposure to toxic substances. In this paper, the cytotoxicity induced by Taxotere® and Chol-Suc-HA-DTX NPs was evaluated in MCF-7, 4T1, A549 and L929 cells using the LDH and MTT assays. Figure 5 presents the dose-responsed histogram for the two assays. It can be seen that the results obtained from the LDH assay were well coordinated with the MTT assay. And cell viability and LDH release after exposure to Taxotere® and Chol-Suc-HA-DTX NPs displayed a dose-dependent manner. The cytotoxicity induced by Chol-Suc-HA-DTX NPs was significantly higher in comparison with Taxotere® at all concentrations (0.0016–1 μg/ml) tested ($P<0.05$), which may be attributed to enhanced intracellular drug levels after internalization of Chol-Suc-HA NPs. The internalization mechanism would be investigated in the following experiment. In addition, we can also find that with the increase of DS of hydrophobic group, the gradually enhanced cytotoxicity to MCF-7, 4T1 and A549 cells induced by Chol-Suc-HA-DTX NPs was observed as described by the Ref (41). As a result, more drugs would be delivered into cancer cells by the Chol-Suc-HA NPs with a higher DS value, resulting in significant cytotoxicity. The IC_{50} values obtained by MTT assay were recorded in Table II. It is apparent that the IC_{50} values of Chol-Suc-HA3-DTX NPs for MCF-7, 4T1 and A549 cells were about 42.5-, 38.9- and 19.2-fold less than that of

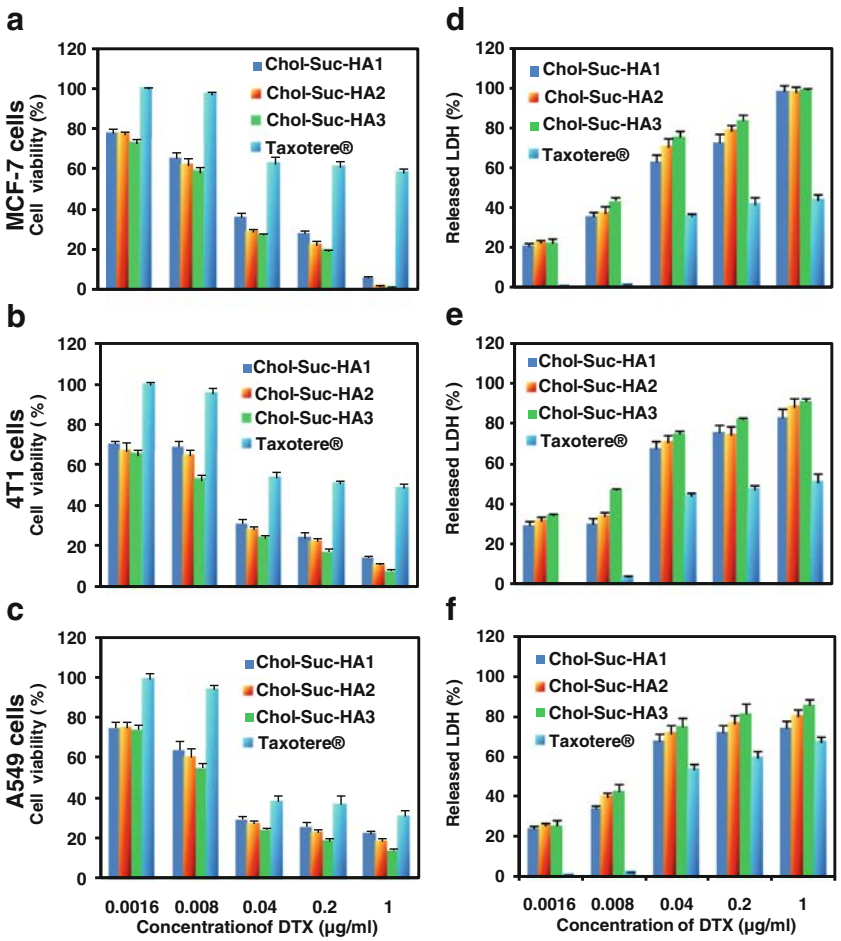

Fig. 5 (**a**-**c**) cell viability and (**d**-**f**) LDH release of MCF-7, 4T1 and A549 cells after treatment with different DTX formulations at various concentrations for 72 h (mean ± S.D., $n = 3$).

Taxotere®, respectively, suggesting that the encapsulation of DTX into Chol-Suc-HA NPs induced a potent anticancer activity. Furthermore, it can be clearly observed that the cytotoxicity of Chol-Suc-HA-DTX NPs to cancer cells was far stronger than that to normal cells (L929), indicating a high selectivity to carcinomatous cell lines.

In Vitro Cellular Uptake

In order to compare the extent of cellular internalization and investigate the mechanism of cellular uptake, CLSM and flow cytometry were used to qualitatively and quantitatively evaluate the cellular uptake of Chol-Suc-HA-C6 NPs and free C6.

Cellular Internalization

As shown in CLSM (Fig. 6a), the fluorescence images obtained from the FITC channel represent the green fluorescence of C6 and the images obtained from the Hoechst channel exhibit the red fluorescence of nuclei stained by Hoechst 33342. In the merged channel of FITC and Hoechst, it is apparent that intracellular fluorescence intensity of Chol-Suc-HA-C6 NPs in three classes of cancer cells was significantly higher than that of free C6. Additionally, the intracellular fluorescence levels of Chol-Suc-HA-C6 NPs were gradually increased with the DS values of hydrophobic moiety increasing. The fluorescence intensity of cells treated with Chol-Suc-HA-C6 NPs or free C6 was also quantitatively determined by flow cytometry.

Table II IC_{50} Values of Different DTX Formulations Against Carcinomatous and Normal Cell Lines

Cell line	Taxotere® (ng/ml)	Chol-Suc-HA1 (ng/ml)	Chol-Suc-HA2 (ng/ml)	Chol-Suc-HA3 (ng/ml)
MCF-7	724.26 ± 2.56	25.61 ± 2.33	19.21 ± 1.89	17.04 ± 1.99
4T1	631.73 ± 3.31	23.17 ± 1.92	18.93 ± 3.03	16.25 ± 2.45
A549	328.18 ± 3.01	28.05 ± 3.76	17.89 ± 2.33	17.05 ± 1.43
L929	480.57 ± 3.23	210.32 ± 3.23	205.14 ± 2.98	214.37 ± 4.01

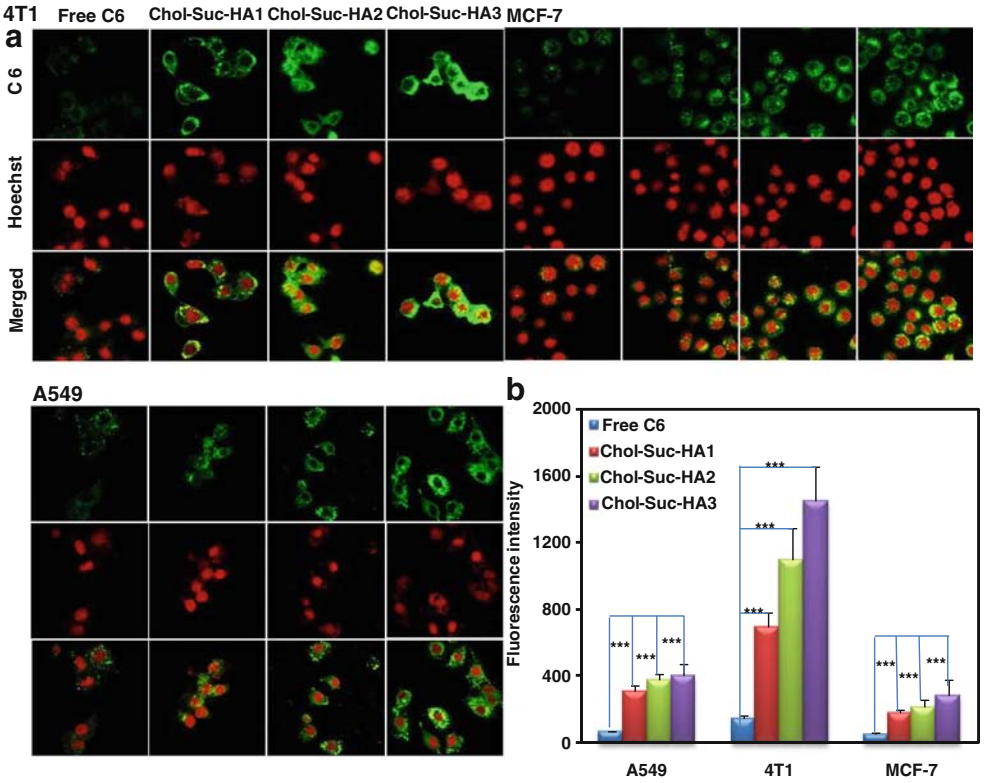

Fig. 6 (**a**) The confocal microscope images (20×) and (**b**) Fluorescence intensity of 4T1, MCF-7 and A549 cells incubated with free C6 and Chol-Suc-HA-C6 NPs for 2 h at 37°C. $^{*}P<0.05$. $^{**}P<0.01$. $^{***}P<0.001$.

The obtained results were in accord with above CLSM observation (Fig. 6b). For example, for 4T1 cells, the intracellular fluorescence intensity was significantly increased from 690.8±92.1 to 1445.9±204.4 with increasing DS values from 8.2 to 25.6%. Combining the results of CLSM and flow cytometry, we could conclude that the higher hydrophobic modification of HA with CHEMS did not affect the binding of HA to CD44 but enhanced the cellular uptake. The amount of C6 encapsulated into three kinds of NPs was almost the same, so the enhanced cellular uptake may be due to the smaller particle size. As evidenced by CLSM, there was notable difference in the intracellular fluorescence intensity of Chol-Suc-HA-C6 NPs and free C6 ($P<0.001$). Particularly for Chol-Suc-HA3-C6 NPs, the intracellular fluorescence level was about 5.4-, 9.7- and 6.1-fold higher than that of free C6 for MCF-7, 4T1 and A549 cells, respectively. Overall, the results obtained from the CLSM and flow cytometry indicated that Chol-Suc-HA NPs with higher DS values would largely enhance the cellular uptake of DTX. The enhancement of cellular uptake may be due to the CD44 receptor-mediated endocytosis.

Investigation on Mechanism of Cellular Uptake

The internalization mechanism was also investigated by performing the following experiments including the competitive inhibition study using HA solution (10 mg/ml), negative control of L929 cells (relatively low level of CD44 expression) and cellular uptake at 4°C. As seen by CLSM and flow cytometry (Fig. 7), pre-treating the $CD44^{+}$ cancer cells (MCF-7, 4T1 and A549) with free HA, the concentration of which in culture medium was markedly higher than that of Chol-Suc-HA conjugates, significantly reduced the internalization of Chol-Suc-HA3-C6 NPs. Only a weak fluorescence signal was observed, indicating that the free HA competitively bound to CD44 and inhibited the uptake of Chol-Suc-HA NPs. In contrast, after the CD44-overexpressed cancer cells were incubated with Chol-Suc-HA3-C6 NPs at 4°C for 2 h, the fluorescence signal was still strong. And as shown in Fig. 7b, d and f, the fluorescence intensity profile at 4°C slightly shifted to the left-side compared with that at 37°C, suggesting there existed significant surface binding. This occurs on non-recyclable receptors (49). In the case of negative control test, no visible difference was observed in the fluorescence intensity of L929 cells treated with single Chol-Suc-HA3-C6 NPs or mixture of free HA solution and NPs, and both of the fluorescence intensity were remarkably lower than that of $CD44^{+}$ cancer cells, indicating a nonspecific cell uptake. Moreover, almost no signals were observed when the L929 cells were incubated with Chol-Suc-HA3-C6 NPs at 4°C. All of above results fully demonstrated that the Chol-Suc-HA NPs could selectively bind to CD44 receptor and efficiently internalize into the three types of cancer cells via CD44 receptor-mediated endocytosis.

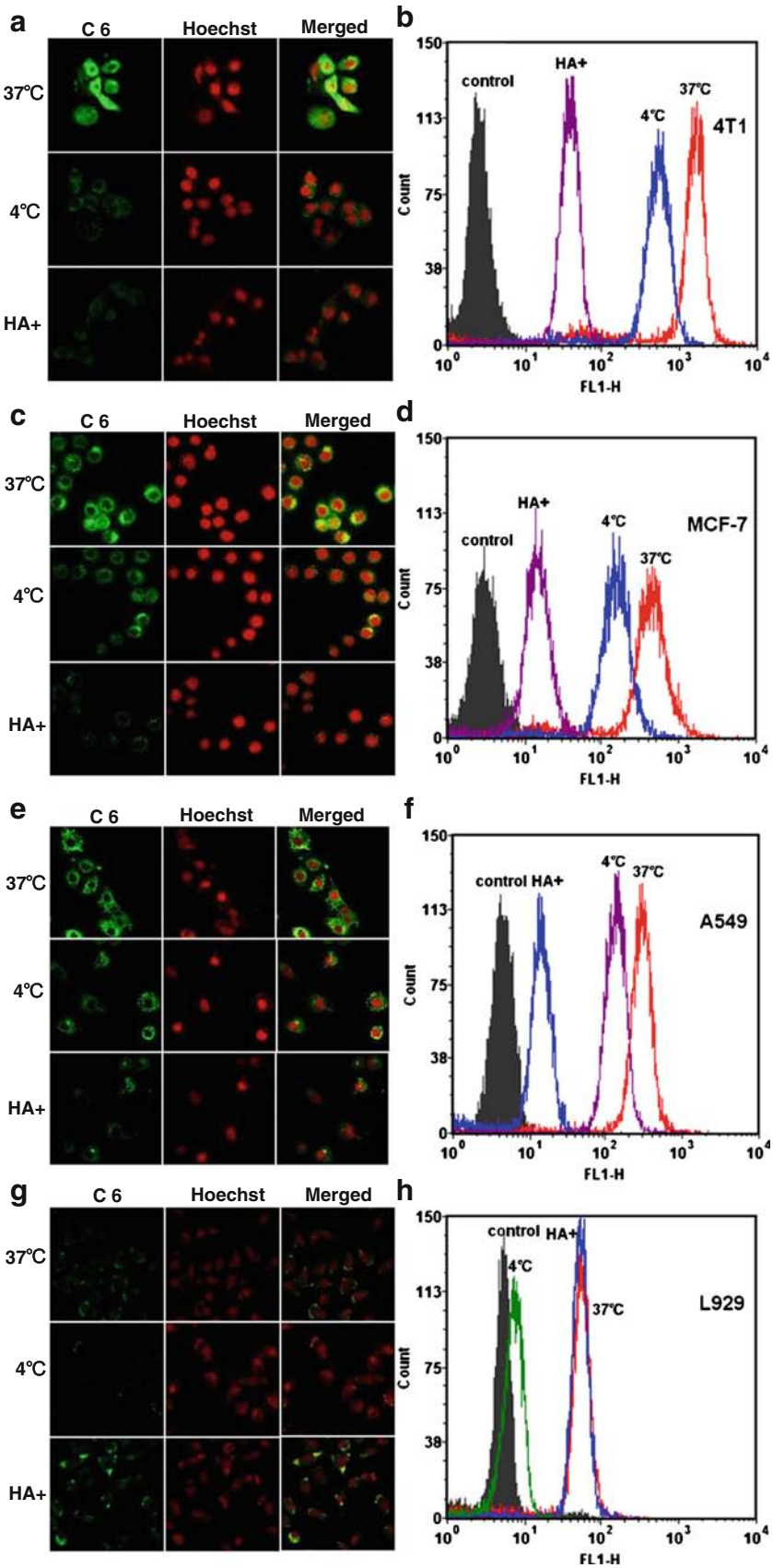

Fig. 7 The confocal microscope images (20×) and flow cytometric curves of 4T1 (**a** and **b**), MCF-7 (**c** and **d**), A549 (**e** and **f**) and L929 (**g** and **h**) cells obtained from the experiments of cell uptake mechanism including the competitive inhibition study using HA solution (10 mg/ml), negative control of L929 cells and cellular uptake at 4°C. In the flow cytometric curves, the cells without any treatment were as a negative control.

The Impact of HA as Hydrophilic Outer-Shell on the Opsonization and M-acrophage Uptake

It was reported that engineering the surface of NPs with hydrophilic polymer including poly(ethylene glycol), poly(N-vinylpyrrolidone), poly(acrylamide) and polysaccharides could reduce the opsonization in the bloodstream and subsequent uptake by mononuclear phagocytic system (MPS). Therefore, the uptake capacity of RAW 264.7 cells for nude CHEMS vesicles as a positive control and Chol-Suc-HA-C6 NPs was investigated by determining the percentage of fluorescence cells using flow cytometry. From the Fig. 8a, it can be seen that there was no significant difference between the uptake level of Chol-Suc-HA NPs by macrophages in the presence or absence of rat plasma ($P>0.05$). Conversely, for the positive control, nude CHEMS vesicles, macrophages uptake was significantly increased after opsonization in rat plasma ($P<0.01$). The percentage of fluorescence cells was up to 82.3% after opsonizing in rat plasma for 30 min, possibly due to electrostatic and hydrophobic interaction between the nude CHEMS vesicles and plasma component. The reduced uptake of Chol-Suc-HA NPs may be in virtue of the HA hydrophilic outer-shell, which could protect the NPs from the opsonization in the bloodstream and the following uptake by MPS, hence resulting in the prolonged circulation time.

In Vivo Pharmacokinetic Evaluation

Surface modification of nanoparticles with hydrophilic polymers, most notably PEG, can provide protection from opsonization and consequently result in increased circulation half-life (50). In order to investigate if the Chol-Suc-HA NPs possess long-circulation property in the blood after systemic administration, the pharmacokinetic evaluation was carried out in SD rats. The mean plasma concentration-time curves as a function of time were presented in Fig. 8b. and corresponding pharmacokinetic parameters were summarized in Table III. As shown in Fig. 8b, there existed significant difference in pharmacokinetic behavior for Taxotere® and Chol-Suc-HA-DTX NPs. DTX from Taxotere® was rapidly eliminated from the circulation system, with less than 200 ng/ml in plasma at 2 h post intravenous injection, whereas encapsulation of DTX into Chol-Suc-HA NPs extended residence time in the blood. Especially for CHOL-SUC-HA3-DTX NPs, the drug concentration in plasma was still more than 1 μg/ml at 12 h post-injection. Formulating DTX in Chol-Suc-HA NPs significantly extended the mean retention time and elimination half-life, increased area under the plasma concentration *versus* time curve and reduced total clearance in comparison with Taxotere® (Table III). Particularly, the $AUC_{0-\infty}$, $MRT_{0-\infty}$ and $t_{1/2}$ for Chol-Suc-HA3-DTX NPs were 47.13 h*mg/L, 9.82 h and 5.56 h, which were 23.9-, 20.9- and 12.6-fold higher than those of Taxotere®, respectively, while the CL for Chol-Suc-HA3 NPs was 22.1-fold lower than that of Taxotere®. The obtained results indicated that Chol-Suc-HA NPs indeed displayed a long-circulation property. The possible explanation could be that HA exposed on the surface of Chol-Suc-HA NPs, similar to PEG, could provide steric stabilization and reduce protein absorption, therefore resulting in the decreased opsonization and prolonged blood circulation time. It is worthy to note that for Chol-Suc-HA1-DTX NPs, the pharmacokinetic parameters were obviously different from those of Chol-Suc-HA2-DTX and Chol-Suc-HA3-DTX NPs. The $AUC_{0-\infty}$, $MRT_{0-\infty}$ and $t_{1/2}$ were only 14.09 h*mg/L, 3.30 h and 2.87 h, which were distinctly lower than those of Chol-Suc-HA2-DTX and Chol-Suc-HA3-DTX NPs. However, the CL value was as high as 0.75 L/h/kg, which was 3-fold higher than that of Chol-Suc-HA3-DTX NPs. The phenomenon that Chol-Suc-HA1-DTX NPs with 8.2% of DS presented a decreased blood circulation time in comparison with other NPs groups could be due to the weak hydrophobic interaction in the hydrophobic inner core, leading to relatively weak stability *in vivo* upon the injection of Chol-Suc-HA1-DTX NPs.

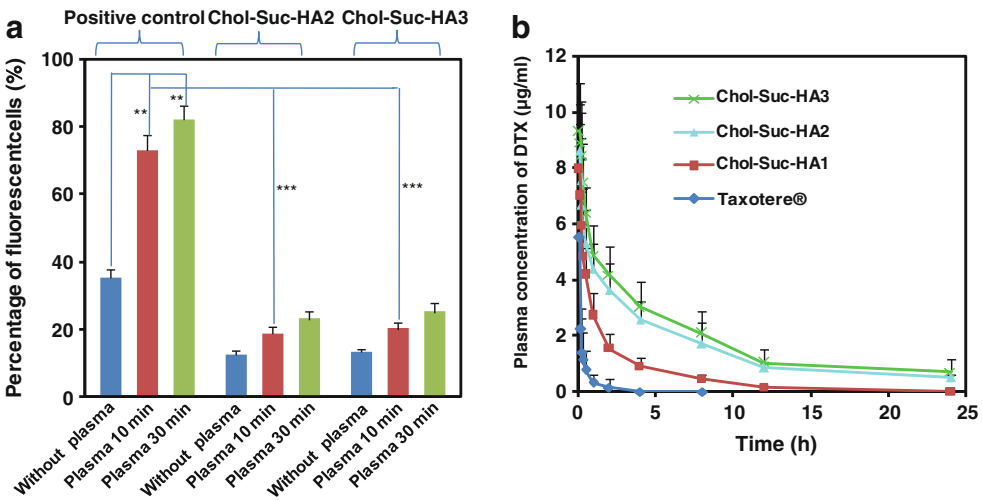

Fig. 8 (**a**) The effect of HA as hydrophilic outer-shell on the uptake of NPs by RAW 264.7. (**b**) Mean concentration-time curves of DTX in rat plasma after intravenous administration of different DTX formulations. Data were expressed as mean ± S.D. ($n=3$). $^{*}P<0.05$. $^{**}P<0.01$. $^{***}P<0.001$.

Table III The Mean Pharmacokinetic Parameters of DTX in SD Rats After Intravenous Administration of Different DTX Formulations

Parameters	Taxotere®	Chol-Suc-HA1	Chol-Suc-HA2	Chol-Suc-HA3
$t_{1/2}$ (h)	0.44 ± 0.08	2.87 ± 0.36	5.37 ± 1.66	5.56 ± 1.05
AUC_{0-24} (h*mg/L)	1.92 ± 0.46	13.42 ± 3.88	38.01 ± 10.45	45.53 ± 12.97
$AUC_{0-\infty}$ (h*mg/L)	1.97 ± 0.47	14.09 ± 3.40	40.99 ± 13.81	47.13 ± 15.19
CL (L/h/kg)	5.31 ± 1.38	0.75 ± 0.22	0.26 ± 0.08	0.24 ± 0.10
MRT_{0-24} (h)	0.35 ± 0.02	2.75 ± 0.13	6.71 ± 0.16	6.80 ± 1.19
$MRT_{0-\infty}$ (h)	0.47 ± 0.10	3.30 ± 0.15	9.69 ± 0.76	9.82 ± 2.80

Bio-Distribution of Chol-Suc-HA NPs Observed by *Ex Vivo* NIRF Imaging

Ex vivo NIRF optical imaging was employed to monitor the tissue distribution and evaluate the tumor-targeting properties of Chol-Suc-HA NPs. From the fluorescence images of dissected tumors and major organs obtained after 24 h post-injection (Fig. 9a), it can be seen that for Chol-Suc-HA2 and Chol-Suc-HA3 NPs, the tumor sites exhibited the strongest fluorescence signal among all the organs (7423 ± 625 and 8527 ± 701, respectively). Compared with Chol-Suc-HA1NPs, the Chol-Suc-HA2 and Chol-Suc-HA3 NPs significantly decreased the DIR accumulation in liver and spleen ($P < 0.05$). This might be explained by the fact that the hydrophilic HA outer-shell protected the NPs from the uptake by the RES. The majority of DIR accumulated in tumors and livers after intravenous injection of Chol-Suc-HA NPs, so the NIRF images and fluorescence intensity of dissected tumors and livers at different time points were shown in Fig. 9b–e. It was clear that the distribution of Chol-Suc-HA NPs in the two tissues was significantly affected by the DS values. For Chol-Suc -HA1 NPs, the fluorescence signal in tumor tissues was extremely lower but significantly higher in livers compared with other two groups ($P < 0.05$). The highest mean fluorescence intensity (MFI) of the tumors was only 4678.5 ± 160, which was 2-fold lower than that of Chol-Suc-HA3 NPs. This may be because the stability of Chol-Suc-HA1 NPs compromised in the bloodstream as evidenced in the experiment of integrity and stability, hence resulting in the lack of long-circulation property and tumor-targeting ability. As for the Chol-Suc-HA2 and Chol-Suc-HA3 NPs, the fluorescence intensity at the tumor sites gradually increased for the first 8 h and slowly decreased over the following 40 h period, possibly due to the long-circulation of Chol-Suc-HA NPs in the bloodstream. From Fig. 9c and d, we can

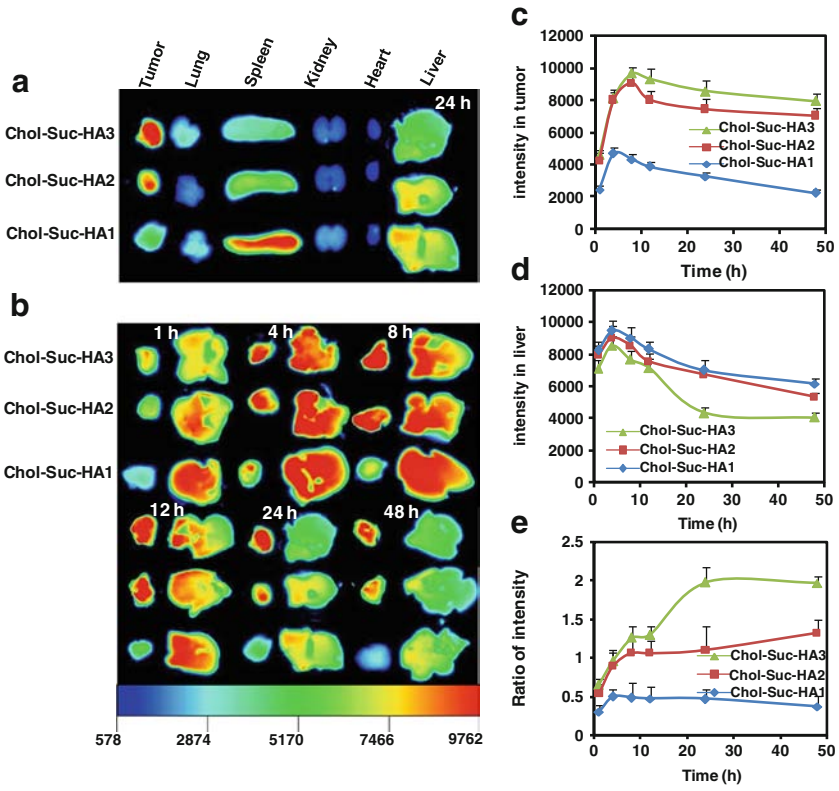

Fig. 9 (**a**) *Ex vivo* fluorescence images of dissected tumors and major organs collected from the tumor-bearing BALB/c mice at 24 h post-injection of different Chol-Suc-HA-DIR NPs. (**b**) The NIRF images of tumors and livers excised from the tumor-bearing BALB/c mice at different time points after intravenous administration of different Chol-Suc-HA-DIR NPs. (**c**) Quantitative fluorescence intensity of tumors from *ex vivo* images. (**d**) Quantitative fluorescence intensity of livers from *ex vivo* images. (**e**) The fluorescence intensity ratio of tumors to livers at different time points after intravenous administration of Chol-Suc-HA-DIR NPs.

find that after 8 h post-injection, the accumulation of Chol-Suc-HA2 and Chol-Suc-HA3 NPs in the tumor tissues was higher than that in livers as indicated by the ratio of fluorescence intensity between tumors and livers (Fig. 9e). The excellent tumor-targeting ability of Chol-Suc-HA2 and Chol-Suc-HA3 NPs could be due to the following reasons: (1) high stability in bloodstream, (2) prolonged blood circulation time, (3) EPR effect, (4) CD44-mediated endocytosis.

In Vivo Antitumor Efficacy

In order to evaluate the antitumor efficacy and systemic toxicity, the tumor volume and body weight of 4T1 tumor-bearing BALB/c mice after intravenous administration of different DTX formulations at the dose of 10 mg DTX/kg were monitored. The dosing schedule was illustrated in Fig. 10a. As shown in Fig. 10b, the Chol-Suc-HA3-DTX NPs group exhibited the highest tumor growth inhibition compared with the saline group ($P<0.001$). After 15-day treatment, the tumor growth rate of Taxotere® group markedly accelerated and was significantly faster compared with Chol-Suc-HA2-DTX and Chol-Suc-HA3-DTX group ($P<0.001$). At the end of the experiment, the tumor was excised and weighed. The tumor inhibition rate (TIR) was calculated. From the Fig. 10e, it was found that the TIR of Chol-Suc-HA2-DTX and Chol-Suc-HA3-DTX group was

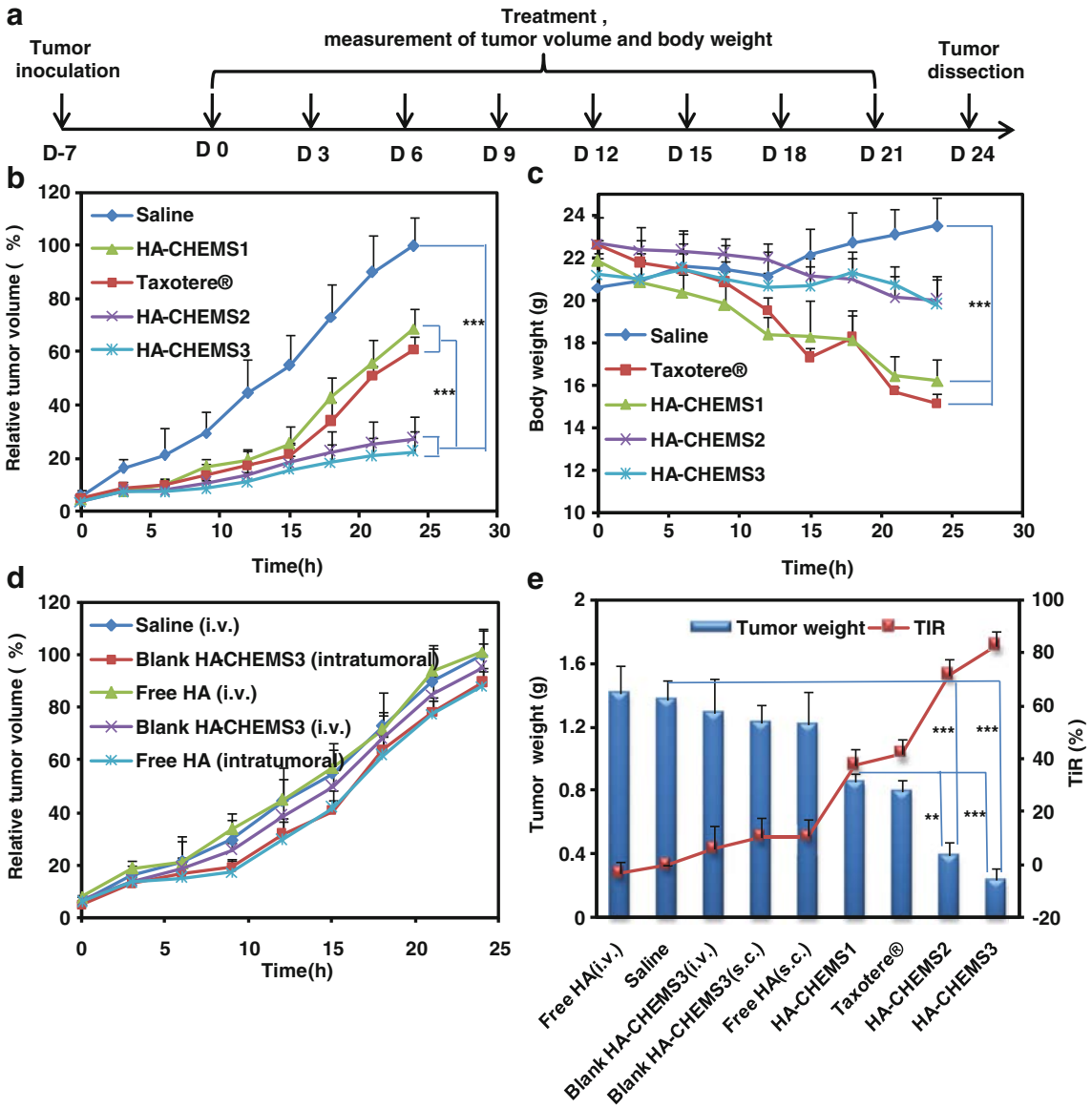

Fig. 10 (**a**) Antitumor activities of Taxotere® and Chol-Suc-HA-DTX NPs in 4T1 tumor-bearing BALB/c mice ($n=6$). (**b**) Body weight change of 4T1 tumor-bearing BALB/c mice after intravenous administration of saline, Taxotere® and Chol-Suc-HA-DTX NPs ($n=6$). (**c**) Changes of tumor volume after injection of blank Chol-Suc-HA3 NPs (i.v.), free HA solution (i.v.), blank Chol-Suc-HA3 NPs (s.c.) and free HA solution (s.c.) ($n=10$). (**d**) Tumor weight and tumor inhibition rate (TIR) at the end of tests. $^{*}P<0.05$. $^{**}P<0.01$. $^{***}P<0.001$.

1.70- and 1.96-fold higher than that of Taxotere® group, respectively. In contrast, the TIR of Chol-Suc-HA1-DTX NPs group was only 37.6%, which was even lower than that of Taxotere® group. The poor therapeutic effect could be due to the loss of NPs integrity after encountering the various plasma components.

Figure 10c presents the variation in body weight of tumor-bearing mice. It can be seen that the Taxotere®-treated mice showed a severe weight loss with the slow decrease during the initial 12 days and then fast reduction. The decrease in body weight was up to 7.5 g. Furthermore, on the 24th day's observation, all of the mice were dead, indicating a serious toxicity to the normal tissue due to drug itself and high concentration of Tween80 formulated in the commercial Taxotere®. Moreover, the body weight of mice treated with Chol-Suc-HA1-DTX NPs also significantly decreased. This may be because the lack of stability and tumor-targeting ability led to the systemic toxicity. However, no significant weight loss was observed after administration of Chol-Suc-HA2-DTX and Chol-Suc-HA3-DTX NPs, indicating that encapsulation of DTX into Chol-Suc -HA NPs with a relatively high DS value could significantly reduce the toxicity to the normal tissue.

The influence of blank Chol-Suc-HA NPs and free HA solution on the tumor growth was also preliminarily investigated. As shown in Fig. 10d, after blank Chol-Suc-HA3 NPs were injected intravenously or intratumorally, there both exhibited a slight inhibition on tumor growth. The TIR was 6.0% for intravenous injection and 10.6% for intratumoral injection. The free HA group after intravenous administration showed no inhibitory effect on the tumor growth, while free HA after intratumoral injection exhibited the similar tumor growth suppression to the blank Chol-Suc-HA3 group. The tumor growth inhibition induced by blank Chol-Suc-HA NPs may be due to many reasons. One of the reasons could be that blank Chol-Suc-HA NPs as exogenous HA interfered with the endogenous CD44-HA interaction which was involved in the tumor growth as reported by Zeng *et al.* (24). However, further investigation on their mechanism of action needs to be pursued.

CONCLUSION

In this study, we successfully prepared the Chol-Suc-HA NPs for targeting delivery of DTX, which exhibited high drug loading, uniform particle size distribution and excellent *in vitro* stability. The DS values of hydrophobic moiety significantly influenced the stability of Chol-Suc-HA NPs in rat plasma. Cellular uptake demonstrated that Chol-Suc-HA NPs would largely enhance the internalization of DTX via CD44 receptor-mediated endocytosis. Compared with Taxotere®, Chol-Suc-HA-DTX NPs displayed remarkably higher cytotoxicity to CD44-positive cancer cells. *In vivo* animal experiments confirmed that Chol-Suc-HA-DTX NPs with relatively high DS values possessed prolonged circulation time, excellent tumor-targeting properties and efficient antitumor effects with extremely low systemic toxicity. In addition, blank Chol-Suc-HA NPs also slightly suppressed the tumor growth. The antitumor mechanism will need to be further investigated. However, a major drawback of CD44 receptor is that it is slowly regenerated on the surface of cells (24–48 h) after being internalized. This drawback will reduce the CD44-mediated uptake of NPs (49,51,52). In the future studies, we will work on solving the problem.

ACKNOWLEDGMENTS AND DISCLOSURES

This work was financially supported by the National Natural Science Foundation of China (NSFC, No.81273447), Hebei Natural Science Foundation of China (HENSF, C2011319007) and special construction projects fund which belongs to "Taishan Scholar——Pharmacy Specially Recruited Experts".

REFERENCES

1. Du C, Deng D, Shan L, Wan S, Cao J, Tian J, *et al.* A pH-sensitive doxorubicin prodrug based on folate-conjugated BSA for tumor-targeted drug delivery. Biomaterials. 2013;34:3087–97.
2. Huo M, Zou A, Yao C, Zhang Y, Zhou J, Wang J, *et al.* Somatostatin receptor-mediated tumor-targeting drug delivery using octreotide-PEG-deoxycholic acid conjugate-modified N-deoxycholic acid-O, N-hydroxyethylation chitosan micelles. Biomaterials. 2012;33:6393–407.
3. Kedar U, Phutane P, Shidhaye S, Kadam V. Advances in polymeric micelles for drug delivery and tumor targeting. Nanomedicine: NBM. 2010;6:714–29.
4. Shen M, Huang Y, Han L, Qin J, Fang X, Wang J, *et al.* Multifunctional drug delivery system for targeting tumor and its acidic microenvironment. J Control Release. 2012;161:884–92.
5. Cui Y, Xu Q, Chow PK-H, Wang D, Wang C-H. Transferrin-conjugated magnetic silica PLGA nanoparticles loaded with doxorubicin and paclitaxel for brain glioma treatment. Biomaterials. 2013;34:8511–20.
6. Wang M, Hu H, Sun Y, Qiu L, Zhang J, Guan G, *et al.* A pH-sensitive gene delivery system based on folic acid-PEG-chitosan–PAMAM-plasmid DNA complexes for cancer cell targeting. Biomaterials. 2013;34:10120–32.
7. Zhang B, Sun X, Mei H, Wang Y, Liao Z, Chen J, *et al.* LDLR-mediated peptide-22-conjugated nanoparticles for dual-targeting therapy of brain glioma. Biomaterials. 2013;34:9171–82.
8. Gaca S, Reichert S, Multhoff G, Wacker M, Hehlgans S, Botzler C, *et al.* Targeting by cmHsp70.1-antibody coated and survivin miRNA plasmid loaded nanoparticles to radiosensitize glioblastoma cells. J Control Release. 2013;172:201–6.
9. Kumari A, Yadav SK, Yadav SC. Biodegradable polymeric nanoparticles based drug delivery systems. Colloids Surf B: Biointerfaces. 2010;75:1–18.
10. Li Y, Wang J, Wientjes MG, Au JLS. Delivery of nanomedicines to extracellular and intracellular compartments of a solid tumor. Adv Drug Deliv Rev. 2012;64:29–39.
11. Prakash S, Malhotra M, Shao W, Tomaro-Duchesneau C, Abbasi S. Polymeric nanohybrids and functionalized carbon nanotubes as drug

delivery carriers for cancer therapy. Adv Drug Deliv Rev. 2011;63: 1340–51.
12. Leeand JY, Spicer AP. Hyaluronan: a multifunctional, megaDalton, stealth molecule. Curr Opin Cell Biol. 2000;12:581–6.
13. Robert L, Robert AM, Renard G. Biological effects of hyaluronan in connective tissues, eye, skin, venous wall. Role in aging. Pathol Biol. 2010;58:187–98.
14. Bullard KM, Kim H-R, Wheeler MA, Wilson CM, Neudauer CL, Simpson MA, *et al.* Hyaluronan synthase-3 is upregulated in metastatic colon carcinoma cells and manipulation of expression alters matrix retention and cellular growth. Int J Cancer. 2003;107:739–46.
15. Itano N, Sawai T, Yoshida M, Lenas P, Yamada Y, Imagawa M, *et al.* Three isoforms of mammalian hyaluronan synthases have distinct enzymatic properties. J Biol Chem. 1999;274:25085–92.
16. Ponta H, Sherman L, Herrlich PA. CD44: from adhesion molecules to signalling regulators. Nat Rev Mol Cell Biol. 2003;4:33–45.
17. Sternand R, Jedrzejas MJ. Hyaluronidases: their genomics, structures, and mechanisms of action. Chem Rev. 2006;106:818–39.
18. Stern R. Hyaluronan catabolism: a new metabolic pathway. Eur J Cell Biol. 2004;83:317–25.
19. Bourguignon LYW. Hyaluronan-mediated CD44 activation of RhoGTPase signaling and cytoskeleton function promotes tumor progression. Semin Cancer Biol. 2008;18:251–9.
20. Toole BP. Hyaluronan: from extracellular glue to pericellular cue. Nat Rev Cancer. 2004;4:528–39.
21. Bourguignon LYW, Wong G, Earle C, Krueger K, Spevak CC. Hyaluronan-CD44 interaction promotes c-Src-mediated twist signaling, MicroRNA-10b expression, and RhoA/RhoC up-regulation, leading to rho-kinase-associated cytoskeleton activation and breast tumor cell invasion. J Biol Chem. 2010;285:36721–35.
22. Götteand M, Yip GW. Heparanase, hyaluronan, and CD44 in cancers: a breast carcinoma perspective. Cancer Res. 2006;66: 10233–7.
23. Kim H-R, Wheeler MA, Wilson CM, Iida J, Eng D, Simpson MA, *et al.* Hyaluronan facilitates invasion of colon carcinoma cells in vitro via interaction with CD44. Cancer Res. 2004;64:4569–76.
24. Bartolazzi A, Peach R, Aruffo A, Stamenkovic I. Interaction between CD44 and hyaluronate is directly implicated in the regulation of tumor development. J Exp Med. 1994;180:53–66.
25. Ghatak S, Misra S, Toole BP. Hyaluronan oligosaccharides inhibit anchorage-independent growth of tumor cells by suppressing the phosphoinositide 3-kinase/Akt cell survival pathway. J Biol Chem. 2002;277:38013–20.
26. Yoshihara S, Kon A, Kudo D, Nakazawa H, Kakizaki I, Sasaki M, *et al.* A hyaluronan synthase suppressor, 4-methylumbelliferone, inhibits liver metastasis of melanoma cells. FEBS Lett. 2005;579:2722–6.
27. Zeng C, Toole BP, Kinney SD, Kuo JW, Stamenkovic I. Inhibition of tumor growth in vivo by hyaluronan oligomers. Int J Cancer. 1998;77:396–401.
28. Heldin C-H, Rubin K, Pietras K, Östman A. High interstitial fluid pressure—an obstacle in cancer therapy. Nat Rev Cancer. 2004;4: 806–13.
29. Zahalka MA, Okon E, Gosslar U, Holzmann B, Naor D. Lymph node (but not spleen) invasion by murine lymphoma is both CD44- and hyaluronate-dependent. J Immunol. 1995;154:5345–55.
30. Luo Y, Bernshaw NJ, Lu Z-R, Kopecek J, Prestwich GD. Targeted delivery of doxorubicin by HPMA copolymer-hyaluronan bioconjugates. Pharm Res. 2002;19:396–402.
31. Luo Y, Ziebell MR, Prestwich GD. A hyaluronic acid-taxol antitumor bioconjugate targeted to cancer cells. Biomacromolecules. 2000;1:208–18.
32. Ganesh S, Iyer AK, Morrissey DV, Amiji MM. Hyaluronic acid based self-assembling nanosystems for CD44 target mediated siRNA delivery to solid tumors. Biomaterials. 2013;34: 3489–502.
33. Kumar A, Sahoo B, Montpetit A, Behera S, Lockey RF, Mohapatra SS. Development of hyaluronic acid–Fe2O3 hybrid magnetic nanoparticles for targeted delivery of peptides. Nanomedicine: NBM. 2007;3:132–7.
34. Lee H, Mok H, Lee S, Oh Y-K, Park TG. Target-specific intracellular delivery of siRNA using degradable hyaluronic acid nanogels. J Control Release. 2007;119:245–52.
35. Yoon HY, Koo H, Choi KY, Lee SJ, Kim K, Kwon IC, *et al.* Tumor-targeting hyaluronic acid nanoparticles for photodynamic imaging and therapy. Biomaterials. 2012;33:3980–9.
36. Laroui H, Grossin L, Léonard M, Stoltz J-F, Gillet P, Netter P, *et al.* Hyaluronate-covered nanoparticles for the therapeutic targeting of cartilage. Biomacromolecules. 2007;8:3879–85.
37. Surace C, Arpicco S, Dufaÿ-Wojcicki AL, Marsaud VR, Bouclier CL, Clay D, *et al.* Lipoplexes targeting the CD44 hyaluronic acid receptor for efficient transfection of breast cancer cells. Mol Pharm. 2009;6:1062–73.
38. Song S, Chen F, Qi H, Li F, Xin T, Xu J et al. Multifunctional tumor-targeting nanocarriers based on hyaluronic acid-mediated and pH-sensitive properties for efficient delivery of docetaxel. Pharm Res 2013;31:1–14.
39. Yu J-M, Li Y-J, Qiu L-Y, Jin Y. Self-aggregated nanoparticles of cholesterol-modified glycol chitosan conjugate: preparation, characterization, and preliminary assessment as a new drug delivery carrier. Eur Polym J. 2008;44:555–65.
40. Upadhyay KK, Bhatt AN, Mishra AK, Dwarakanath BS, Jain S, Schatz C, *et al.* The intracellular drug delivery and anti tumor activity of doxorubicin loaded poly(γ-benzyl l-glutamate)-b-hyaluronan polymersomes. Biomaterials. 2010;31:2882–92.
41. Liu Y, Sun J, Cao W, Yang J, Lian H, Li X, *et al.* Dual targeting folate-conjugated hyaluronic acid polymeric micelles for paclitaxel delivery. Int J Pharm. 2011;421:160–9.
42. Itano N. Simple primary structure, complex turnover regulation and multiple roles of hyaluronan. J Biochem. 2008;144:131–7.
43. Stern R, Asari AA, Sugahara KN. Hyaluronan fragments: an information-rich system. Eur J Cell Biol. 2006;85:699–715.
44. Chao KL, Muthukumar L, Herzberg O. Structure of human hyaluronidase-1, a hyaluronan hydrolyzing enzyme involved in tumor growth and angiogenesis. Biochemistry. 2007;46:6911–20.
45. Choi KY, Yoon HY, Kim J-H, Bae SM, Park R-W, Kang YM, *et al.* Smart nanocarrier based on PEGylated hyaluronic acid for cancer therapy. ACS Nano. 2011;5:8591–9.
46. Fraser J, Laurent T, Laurent U. Hyaluronan: its nature, distribution, functions and turnover. J Intern Med. 1997;242:27–33.
47. Laurentand TC, Fraser J. Hyaluronan. FASEB J. 1992;6:2397–404.
48. Chen H, Kim S, He W, Wang H, Low PS, Park K, *et al.* Fast release of lipophilic agents from circulating PEG-PDLLA micelles revealed by in vivo forster resonance energy transfer imaging. Langmuir. 2008;24:5213–7.
49. Almalik A, Karimi S, Ouasti S, Donno R, Wandrey C, Day PJ, *et al.* Hyaluronic acid (HA) presentation as a tool to modulate and control the receptor-mediated uptake of HA-coated nanoparticles. Biomaterials. 2013;34:5369–80.
50. Gaucher G, Asahina K, Wang J, Leroux J-C. Effect of poly (N-vinylpyrrolidone)-block-poly (D, L-lactide) as coating agent on the opsonization, phagocytosis, and pharmacokinetics of biodegradable nanoparticles. Biomacromolecules. 2009;10:408–16.
51. Aguiar DJ, Knudson W, Knudson CB. Internalization of the hyaluronan receptor CD44 by chondrocytes. Exp Cell Res. 1999;252:292–302.
52. Ouasti S, Kingham PJ, Terenghi G, Tirelli N. The CD44/integrins interplay and the significance of receptor binding and re-presentation in the uptake of RGD-functionalized hyaluronic acid. Biomaterials. 2012;33:1120–34.